Optical constants of highly stretch-oriented poly(*p*-phenylene-vinylene): A joint experimental and theoretical study

D. Comoretto and G. Dellepiane
Istituto Nationale per la Fisica della Materia, Dipartimento di Chimica e Chimica Industriale, Università di Genova via Dodecaneso 31, I-16146 Genova, Italy

F. Marabelli
INFM, Dipartimento di Fisica ''A. Volta,'' Università degli Studi di Pavia, via Bassi 6, I-27100 Pavia, Italy

J. Cornil and D. A. dos Santos
Service de Chimie des Matériaux Nouveaux, Centre de Recherche en Electronique et Photonique Moléculaires, Université de Mons-Hainaut, Place du Parc 20, B-7000 Mons, Belgium

J. L. Brédas
Service de Chimie des Matériaux Nouveaux, Centre de Recherche en Electronique et Photonique Moléculaires, Université de Mons-Hainaut, Place du Parc 20, B-7000 Mons, Belgium and Department of Chemistry, University of Arizona, Tucson, Arizona, 85721-0041

D. Moses
Institute for Polymers and Organic Solids, University of California at Santa Barbara, Santa Barbara, California 93106-5090
(Received 7 March 2000)

We have determined the frequency dispersion of the anisotropic complex optical constants of highly stretch-oriented poly(*p*-phenylene-vinylene) chains from Kramers-Kronig transformation of polarized near-normal-incidence absolute reflectivity data, inversion of polarized reflectance and transmittance measurements, and spectroscopic ellipsometry. The spectroscopic data are discussed in comparison to the results provided by correlated quantum-chemical calculations. On this basis, we assign the nature and polarization of the optical transitions in poly(*p*-phenylene-vinylene) chains.

I. INTRODUCTION

Among conjugated polymers, poly(*p*-phenylene-vinylene) (PPV) and its soluble derivatives attract a great deal of attention for their use as active elements in the production of low-cost, light, and flexible optoelectronic devices such as light-emitting diodes (LED's), photovoltaic cells, and lasers.[1] The development of the organic LED technology has now reached the stage of commercialization under the form of backlights in flat panel displays.[2] In parallel, this research has stimulated new studies in the field of amplified optically pumped stimulated emission in thin organic films, with the perspectives of achieving electrically pumped solid-state polymer lasers.

In spite of the impressive technical performances reached for the LED devices, many fundamental aspects of the electronic and optical properties of the materials are not yet fully resolved. For instance, the frequency dispersion of the complex refractive index ($\tilde{n}=n+ik$) of PPV has not been studied so far in great detail, and the assignment of the optical transitions and their polarization in this conjugated polymer is still under debate. The knowledge of $\tilde{n}$ is very important to characterize the propagation and losses of lasing modes in waveguides, rings, and microcavities.[3–12] In multilayer LED devices, the real part of the refractive index of the polymer film defines the amount of light reflected back into the device, thus preventing its escape. The value of n is therefore a critical parameter governing the external quantum efficiency in LED's.[13–15]

The influence of side groups, chain-end effects, interchain interactions, and polarization of the medium has been invoked to rationalize the nature and polarization of the optical transitions above the lowest absorption band in PPV and in its substituted derivatives.[16–29] The absence of a unified picture is mainly due to the lack of high-optical-quality oriented samples of PPV that would allow for an unambiguous experimental determination of the anisotropic optical response of the material. Recently, the assignment of the optical transitions in PPV has been refined on the basis of reflectivity measurements performed on highly stretch-oriented *unsubstituted* PPV samples.[30] Additional insight was afforded by polarized absorption spectra of oriented poly[2-methoxy, 5-(2′-ethyl9-hexyloxy)*p*-phenylene-vinylene] (MEH-PPV) blended in a polyethylene matrix.[31]

In this paper, we present a spectroscopic determination of the anisotropic optical constants of highly stretch-oriented PPV by means of Kramers-Kronig transformation of the reflectivity spectra, inversion of the reflectance and transmittance spectra over the transparent spectral region, and spectroscopic ellipsometry. The experimental data are compared to the results provided by correlated quantum-chemical calculations. The very good agreement between the experimental and theoretical spectra allows to shed light on the polarization properties of both the real and imaginary parts of the dielectric constant and refractive index. On this basis, the

controversial origin of the high-energy transitions in the optical spectra of PPV and substituted derivatives is also discussed.

II. EXPERIMENT

The stretch-oriented PPV samples were prepared according to the procedure reported in Ref. 32. The stretching ratio is 3 and the thickness of the film is between 17 and 18 μm, as measured by a Mitutoyo comparator in several different positions of the sample. The optical reflectance (R) and transmittance (T) spectra were measured with a double-grating, Varian model Cary 5E spectrometer between 0.4 and 6.9 eV (3000 and 180 nm). The light was linearly polarized by a Glan-Taylor prism operating in the 250–3000-nm range. We used the partially polarized light of the spectrophotometer for the measurements in the 180–250-nm range, which is not covered by our polarizers. The spectra have a resolution of about 0.5 nm and are collected in 3 s averaging time. A Harrick depolarizing filter was used to avoid the effect of the dependence of the detector response on the polarization of the light. In order to define the direction of polarization parallel to the chain axis, we aligned the polarizer with respect to the samples in such a way that the optical signal associated with the lowest absorption band was maximized. The perpendicular component can then be obtained by rotating the polarizer by 90°. We used an aluminum mirror, whose absolute reflectivity was previously and independently measured using a VW accessory as a reference for the reflectance measurements. The relative reflectance of the sample is then normalized to the reflectivity of the mirror to obtain the absolute values of the anisotropic reflectance of our films.

Spectroscopic ellipsometry measurements were also performed on the samples with incidence angles of 65° and 70° using a Sopra Model No. ES4G ellipsometer with rotating polarizer (RPE) in the spectral range 1.4–5 eV. We aligned the incidence plane with respect to the chain axes by maximizing the intensity of the lowest absorption band. For each incidence angle, two measurements with the incidence plane parallel and perpendicular to the polymer chains, respectively, are performed. Note that imperfections in the flatness of the sample as well as a small misalignment of the chains with respect to the optical axis can affect the ellipsometric signal, which is a complicated convolution of the optical response along the two axes defined on the sample surface. Since the signal obtained for the polarization perpendicular to the chain is much lower than that associated with the parallel component for the lowest absorption band, a small error can also be unintentionally introduced during the deconvolution of the signal. Measurements performed at two different incidence angles (for which the ratio between the two anisotropic contributions are different) can help in overcoming such problems.

The Raman spectra were recorded with a Dilor Model Labram Raman spectrometer equipped with a He-Ne laser ($\lambda_{exc} = 632.8$ nm).

During the ellipsometric, reflectance/transmittance, and Raman measurements, the sample was maintained under dry nitrogen gas flux in order to prevent its photooxidation. Furthermore, all the measurements were repeated in order to assess their reproducibility.

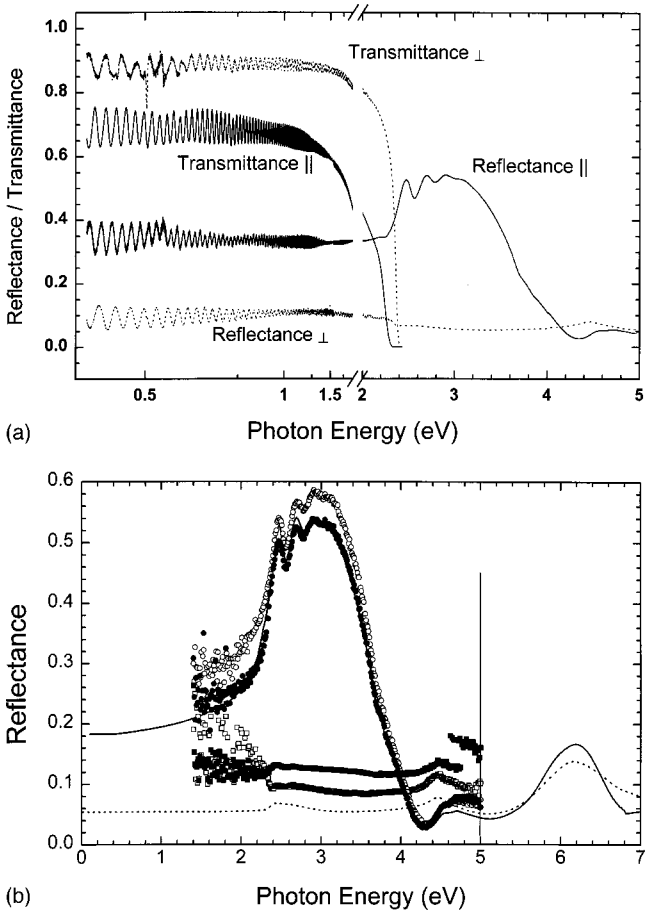

FIG. 1. (a) Room-temperature polarized reflectance and transmittance spectra of highly stretch-oriented PPV. The solid and dashed lines refer to the parallel and perpendicular components, respectively. (b) Calculated reflectance spectrum from n and k deduced by KK transformation (solid and dashed lines for the parallel and perpendicular components, respectively); spectroscopic ellipsometry (filled and open symbols for the 65° and 70° incidence angle, respectively; circles and squares for the parallel and perpendicular components, respectively). The vertical bar at 5 eV separates the spectral region where the light is polarized by the Glan-Taylor prism (below 5 eV) from the spectral range where the partially polarized light of the spectrophotometer is used to record the spectra (above 5 eV).

III. RESULTS

Figure 1(a) shows the room-temperature near-normal-incidence absolute reflectance spectra of oriented PPV for polarizations parallel and perpendicular to the chain direction. For the parallel component, a strong signal associated with the 0-0 vibronic transition of the lowest absorption band is observed at 2.48 eV (500 nm) and is followed by a well-resolved vibronic progression with peaks at 2.70 and 2.95 eV (460 and 420 nm, respectively) and by a shoulder at 3.10 eV (400 nm). We also detect a weak structure around 2.18 eV (570 nm). On the high-energy side of the spectrum, a low-intensity peak is observed at 4.71 eV (263.5 nm) accompanied by a shoulder at 4.56 eV (272 nm). Moreover, a change in the slope of the spectrum occurs around 3.76 eV (330 nm), thus indicating the presence of other transitions. The low-energy part of the spectrum (below 2 eV) is dominated by a

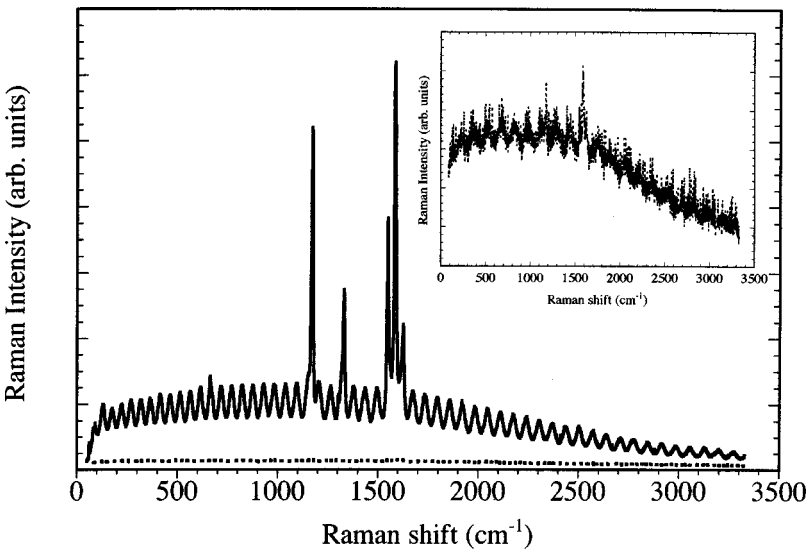

FIG. 2. Raman spectrum of highly stretch-oriented PPV. The solid and dashed lines correspond to the (z,z) and (x,z) components, respectively. We show in the inset the magnification of the (x,z) spectrum.

series of fringes due to the interference of the light reflected by the front and back surfaces of the film.

The lowest optical transition and its vibronic satellites are practically not detectable along the perpendicular component of the reflectance spectrum. This confirms that the polymer chains are very well oriented and the misalignment angle is very small. A single absorption feature is observed in the uv spectral region at 4.47 eV (277.5 nm) for the perpendicular component. Below 2.4 eV, a reflectance signal arising from the contribution of the back surface and a series of interference fringes are clearly detected. Changes in the path of these fringes with respect to that observed for the parallel component points to the anisotropy of the refractive index.

Figure 1(a) also reports the polarized transmittance spectra of PPV up to 2.4 eV (about 500 nm) beyond which the film is no longer transparent to the radiation. Interference fringes are also detected in these spectra.

Figure 2 shows the Raman spectra of the highly oriented PPV chains obtained for the electric field of the exciting radiation polarized both parallel (z) and perpendicular (x) to the chain axis. We focus here on the scattered radiation polarized along the main chain axis. In the (z,z) configuration (where the first term in parentheses refers to the polarization of the exciting radiation and the second to the polarization of the scattered radiation), Raman lines are detected at 1171 (0.145), 1328 (0.165), 1548 (0.192), 1583 (0.196), and 1627 cm^{-1} (0.202 eV) and are superimposed to a broad and sinusoidal photoluminescence background arising from the preresonant absorption of the 632.8-nm laser line. The structured background prevents the observation of the weak Raman bands reported by other authors.[33,34] In the (x,z) configuration (see the enlargement in the inset of Fig. 2), the Raman lines have a much lower intensity due to the high degree of orientation of the polymer chains, and a sinusoidal background is again detected. Since the exciting radiation is focused on the surface of the sample, we suggest that these oscillations could be attributed to the interference between the photoluminescence emitted at the surface and that emitted there but reflected by the back surface of the sample. In fact, at this wavelength, the penetration optical path depth, estimated as the inverse of the absorption coefficient (see next section) is about 77 and 220 μm for the parallel and perpendicular polarizations, respectively. These values are much larger than the sample thickness, thus allowing the light reflection from the back surface of the sample. This interpretation of the structured background of the Raman spectra is further supported by the comparison of the fringes there detected with those observed in the transmittance and reflectance spectra in the same spectral range. Since for each polarization the number of fringes detected in the three kinds of spectra is identical (within the experimental uncertainty), we argued that interference effects play a role in the explanation of the data. Moreover, the different number of fringes observed for the two polarization configurations confirms this interpretation and points out the strong optical birefringence of the sample.

IV. DATA ANALYSIS: DETERMINATION OF THE OPTICAL CONSTANTS

We have determined the complex optical constants of the material both from the R and T spectra and from spectroscopic ellipsometry. Different kinds of data analysis were carried out on the R and T spectra in order to extract the dielectric functions along the parallel and perpendicular directions, both below and above the energy of the lowest optical absorption band.

In order to evaluate n below 1.6 eV, where the sum of R and T is within the experimental error equal to 1, a numerical inversion of the R and T spectra has been performed by assuming $k=0$ and the sample to be flat with parallel surfaces and by modeling its reflectance and transmittance from the sum of the internal reflection components.[35,36] The values of n used as input for the numerical inversion are obtained from the pronounced interference fringes observed in the transmittance and/or reflectance spectra by the well-known formula:

$$\frac{1}{\lambda_k}-\frac{1}{\lambda_{k+1}}=\frac{1}{2nd}, \tag{1}$$

where λ_{k+1} and λ_k are the wavelengths of two successive maxima (or minima) and d is the measured sample thickness. In this spectral region, the model provides the n spectra reported in Figs. 3 and 4 (open squares) as well as the sample

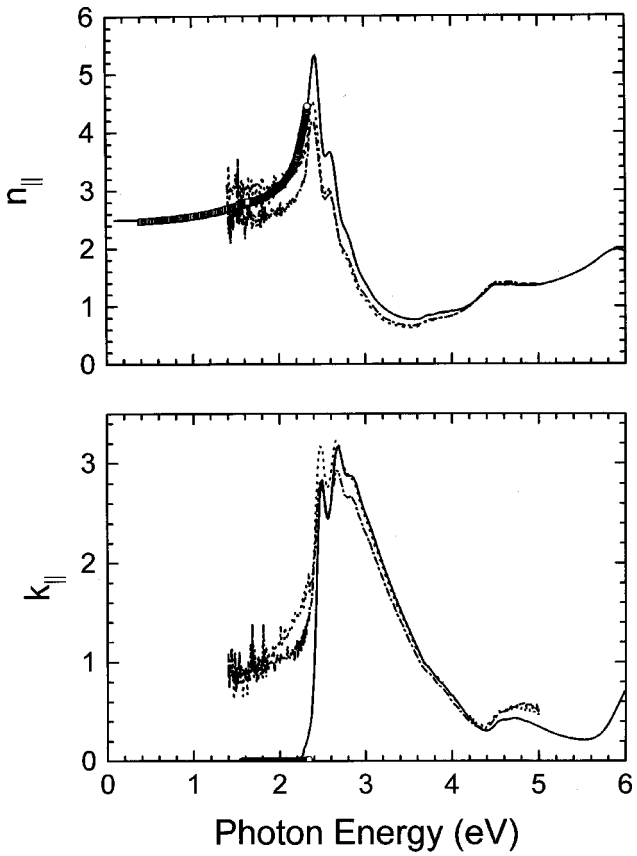

FIG. 3. Frequency dispersion of the parallel component of the real (upper panel) and imaginary part (lower panel) of the refractive index of PPV (solid line from KK analysis; open symbols from the inversion procedures of R and T; dotted line from ellipsometry at 70° incidence angle; dot-dashed line from ellipsometry at 65° incidence angle).

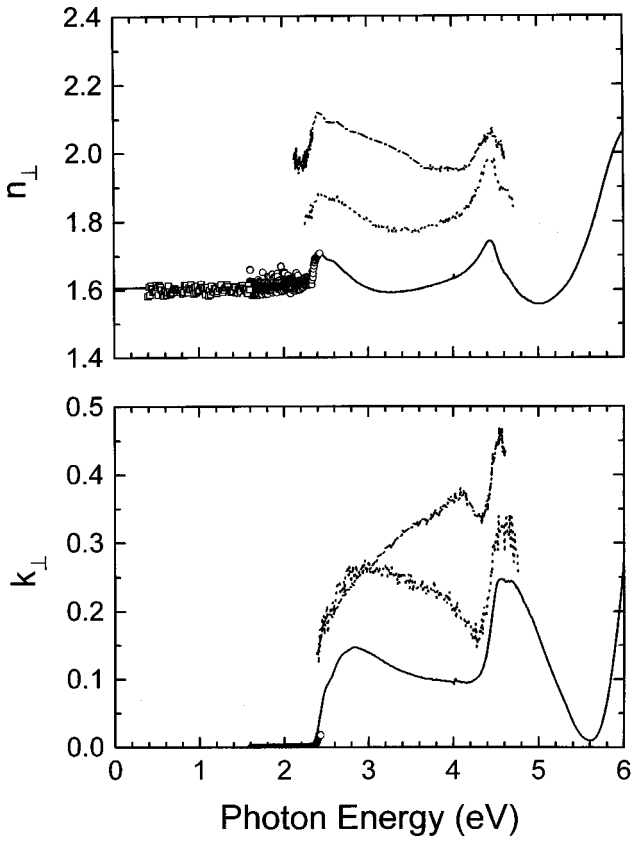

FIG. 4. Frequency dispersion of the perpendicular component of the real (upper panel) and imaginary part (lower panel) of the refractive index of PPV (solid line from KK analysis; open symbols from the inversion procedures of R and T; dotted line from ellipsometry at 70° incidence angle; dot-dashed line from ellipsometry at 65° incidence angle).

thickness (17–18 μm) in very good agreement with the independently measured values. The advantage of using such a simulation model instead of the more simple calculations based on the interference fringes is justified by the fact that we can separately evaluate the refractive index n which governs the absolute values of reflectance and transmittance, and the sample thickness, whose product with n determines the spectral path of the fringes. The coincidence of the measured and derived values of the sample thickness is a check of the quality of our data. In the model, partial coherence has to be considered since a fully coherent transparent system would lead to large interference fringes with extrema at 0 and $R_{\max}=[(n^2-1)/(n^2+1)]^2$ for the reflection and at $1-R_{\max}^2$ and 1 for the transmittance. The absence of such features in our spectra is probably related to small inhomogeneity in the thickness of the samples and/or to slight curvatures of the surface.

The same model was also used without imposing the condition $k=0$. In this way, $\tilde{n}$ can be determined in the full spectral range where T is available, thus allowing for the description of the increase in the absorption coefficient at the absorption edge where the approximation $k=0$ is no longer valid. The values of n and k obtained by means of this simulation model account very well for the interference fringes and give $k=0$ below 1.6 eV, according to the first procedure used. These results are also reported in Figs. 3 and 4 as open circles.

The numerical inversion procedures of R and T lead to values of n at very low frequency that are close to 2.5 and 1.6 for polarizations parallel and perpendicular to the polymer chains, respectively. These values progressively increase as the incident photon energy shifts towards the lowest optical absorption band. The frequency dispersion of the anisotropic dielectric constant deduced from these data, more directly related to the electronic structure of the materials in comparison to $\tilde{n}$, is reported in Figs. 5 and 6.

Above the absorption edge, the measured reflectance corresponds to the near-normal reflectivity (i.e., the reflectance of a semi-infinite material). With an appropriate extrapolation of the data beyond the highest and lowest measured energies, we performed a Kramers-Kronig (KK) analysis to calculate the dispersion of the complex dielectric function. The high-energy tails added to the measured spectra have to ensure that the value of n in the near-infrared (NIR) region is compatible with that obtained by the R and T inversion procedure. Figure 1(b) shows the reflectivity spectrum of the PPV films used for the KK analysis. For energies below the lower limit of the experimental range, the extrapolation is made under the form of a straight line through a constant value for both polarizations, thereby neglecting the signature of phonons. The choice of the high-energy extrapolation curve is much more delicate. Usually, the simplest approximation consists in using data from the literature; however, to the best of our knowledge, such data are not available for

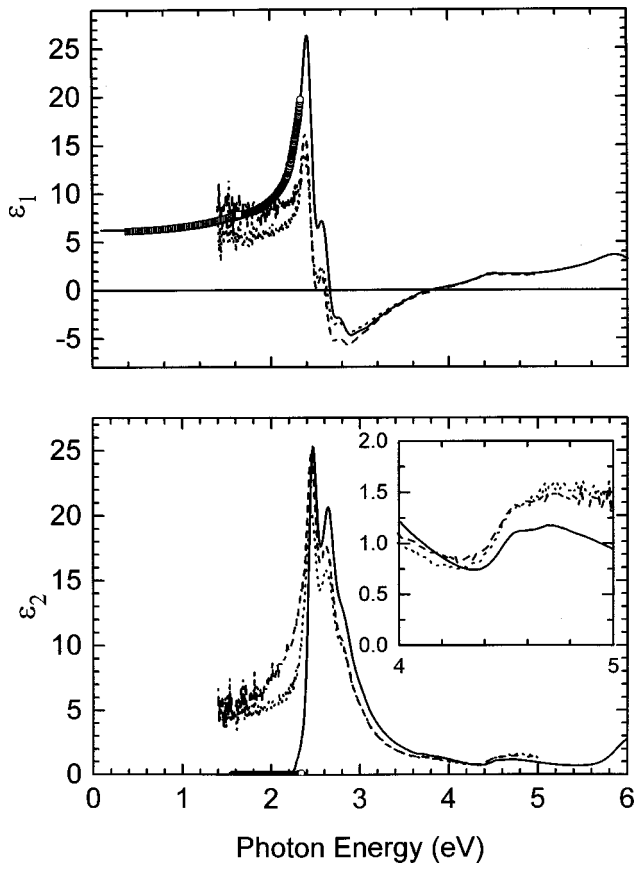

FIG. 5. Frequency dispersion of the parallel component of the real (upper panel) and imaginary part (lower panel) of the dielectric constant of PPV (solid line from KK analysis; open symbols from the inversion procedures of R and T; dotted line from ellipsometry at 70° incidence angle; dot-dashed line from ellipsometry at 65° incidence angle).

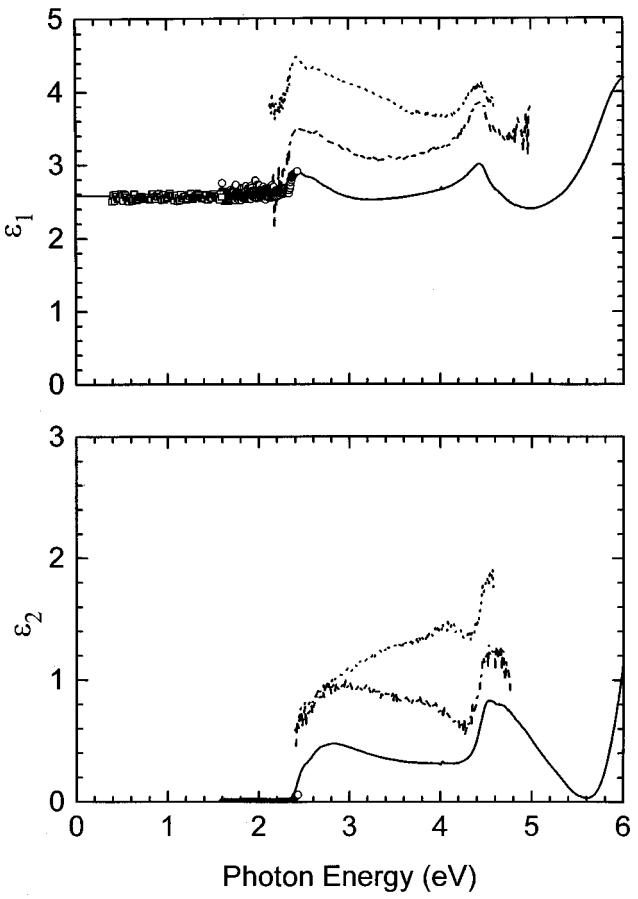

FIG. 6. Frequency dispersion of the perpendicular component of the real (upper panel) and imaginary part (lower panel) of the dielectric constant of PPV (solid line from KK analysis; open symbols from the inversion procedures of R and T; dotted line from ellipsometry at 70° incidence angle; dot-dashed line from ellipsometry at 65° incidence angle).

PPV. We have extended the spectra above 5 eV on the basis of measurements performed with partially polarized light,[30] keeping in mind that the absolute values of the optical functions may not be fully reliable in the high-energy range. The extrapolation of the spectra above 6.5 eV was first based on the formula $R=R_0(\omega/\omega_0)^s$, where R_0 is the reflectivity at the frequency ω_0, which usually corresponds to the highest energy probed by the experimental measurements and where the exponent s is generally chosen between 2 and 4.[37] We have failed when trying to adjust this parameter in order to ensure that the refractive index obtained by the KK analysis coincides in the transparency region with the results obtained by R and T inversion. This demonstrates the existence of additional optical transitions above 6.5 eV, as suggested by electron-energy-loss spectroscopy (EELS) data on oriented PPV showing optical transitions above 10 eV.[38] A simple linear extrapolation of the reflectance spectra between 6.5 and 15 eV yields a good match between the dispersion of n in the NIR spectral range obtained by KK analysis and that provided by R and T inversion. The results are weakly affected by changes in the slope of this linear extrapolation.

There is a major concerning with the kind of extrapolation used here since different choices might lead to changes in the absolute value of the optical constants and shape behavior at critical points such as at the absorption edge (where the numerical KK analysis suffers from a lack of resolution). Nevertheless, in spite of the integration procedures, the local character of the KK analysis does not affect very much the spectral behavior of the optical constants, except for the energy ranges close to the extrapolated regions. If optical features are not properly accounted for by the extrapolation beyond the energy range covered by the experimental measurements, a ''tail'' effect can introduce an additional background to the high-energy part of the calculated dispersions. This effect might be detrimental for our analysis due to the existence of optical features with different polarizations that overlap in the energy range above 4.4 eV. Our different approaches lead us to the conclusion that the shape of the spectra above 6 eV (Ref. 38) does not affect the KK analysis significantly and hence the quality of the data reported in this work. The results of the KK analysis are reported in Figs. 3–6 and compared in the low-energy range to those obtained from the R and T inversion technique. Figures 3 and 4 (5 and 6) refer to the dispersion of the parallel and perpendicular components of n and k (ε_1 and ε_2), respectively.

The reliability of the KK analysis is further supported by analyzing the ellipsometric data. Ellipsometry has two main advantages with respect to reflectance measurements: (i) it is less sensitive to the surface roughness and to light-scattering

effects; (ii) it allows at each frequency the simultaneous determination of two physical parameters, i.e., n and k or n and d. In the case of bulk samples, this allows the determination of both the real and imaginary parts of the dielectric function without going through a complex treatment such as a KK analysis. The main drawback with anisotropic samples is that the measured ellipsometric functions $\tan(\psi)$ and $\cos(\Delta)$ are related both to the incidence angle and the anisotropic reflectance coefficient for polarizations parallel and perpendicular to the incidence plane. The parameters have thus to be deconvolved from a set of measurements performed with different orientations of the sample. Assuming that the anisotropy is uniaxial and that the optical axis of the sample lies on the surface and can be oriented either parallel or perpendicular to the incidence plane, the formalism is simplified and leads to[35]

$$\tan(\psi^{\parallel,\perp})\exp(i\Delta^{\parallel,\perp}) = \frac{r_p^{\parallel,\perp}}{r_s^{\parallel,\perp}}, \tag{2}$$

$$r_s^{\parallel} = \frac{\cos\phi - \sqrt{(\tilde{n}_{\perp}^2 - \sin^2\phi)}}{\cos\phi + \sqrt{(\tilde{n}_{\perp}^2 - \sin^2\phi)}},$$

$$r_p^{\parallel} = \frac{\tilde{n}_{\parallel}\tilde{n}_{\perp}\cos\phi - \sqrt{(\tilde{n}_{\perp}^2 - \sin^2\phi)}}{\tilde{n}_{\parallel}\tilde{n}_{\perp}\cos\phi + \sqrt{(\tilde{n}_{\perp}^2 - \sin^2\phi)}}, \tag{3}$$

$$r_s^{\perp} = \frac{\cos\phi - \sqrt{(\tilde{n}_{\parallel}^2 - \sin^2\phi)}}{\cos\phi + \sqrt{(\tilde{n}_{\parallel}^2 - \sin^2\phi)}},$$

$$r_p^{\perp} = \frac{\tilde{n}_{\parallel}^2\cos\phi - \sqrt{(\tilde{n}_{\perp}^2 - \sin^2\phi)}}{\tilde{n}_{\parallel}^2\cos\phi + \sqrt{(\tilde{n}_{\perp}^2 - \sin^2\phi)}}. \tag{4}$$

$r_p^{\parallel,\perp}$ and $r_s^{\parallel,\perp}$ are the (complex) Fresnel reflection coefficients for light polarized parallel (p) or perpendicular (s) to the incidence plane, respectively, with the optical axis of the sample being parallel ($\parallel$) or perpendicular ($\perp$) to this plane; $\tilde{n}_{\parallel}$ and $\tilde{n}_{\perp}$ are the complex refractive indices along the extraordinary (parallel to the chains) and ordinary (perpendicular to the chains) axes, respectively; ϕ is the angle between the normal to the surface of the sample and the direction of propagation of the incident beam. The detector is fixed at the angle $-\phi$ in the incidence plane.

On the basis of a couple of ellipsometric measurements performed for the two orientations of the sample at a fixed ϕ, we can numerically invert Eqs. (3) and (4) and extract $\tilde{n}_{\parallel}$ and $\tilde{n}_{\perp}$. Since these nonlinear equations provide multiple solutions, we have selected the correct values by comparing the ellipsometric results obtained at different incidence angles with those afforded by a KK analysis. The constraint of having similar results from ellipsometric measurements performed at different ϕ angles also requires the conversion of the nominal value of ϕ into an effective one (67° instead of 65° and 71° instead of 70°). This partially compensates the possible misalignment of the sample with respect to the beam, which can lead to a deep modulation of the ellipsometric response. The intrinsic small misalignment of the chains in our sample can also affect the results, particularly in the direction associated to the lowest optical reflectance.

The complex refractive index determined by ellipsometry is reliable only in the spectral region where the sample can be considered as a bulk. Below the absorption edge at 2.3 eV, a depolarized light component is superimposed on the ellipsometric signal due to the reflection on the back surface of the sample. This additional component strongly modulates the values of the ellipsometric functions, particularly $\tan(\psi)$, and affects the spectra at the absorption edge. We report in Figs. 3–6 the ellipsometric data for the two polarizations and compare them to the corresponding frequency dispersions obtained by R and T inversion and KK analysis.

The agreement between the KK and ellipsometric results is satisfactory for the parallel component of the optical functions for energies above the lowest optical transition where the sample can be considered as a bulk. Changes in the signal as a function of the incident angle and significant noise can be detected at the absorption onset due to the contribution of the back surface of the sample. The larger deviations between the absolute values of ε_2 (or k) determined by the two methods in the high-energy range (see inset of Fig. 5) can be attributed to light-scattering effects (due to surface imperfections), which partially attenuate the measured reflectance. This discrepancy is clearly seen in Fig. 1(b) that compares the measured reflectivities to those estimated from the ellipsometric data.

The comparison of the results obtained with the different techniques is less meaningful for the perpendicular polarization since the weakness of the signals makes all the measurements more sensitive to any small experimental or sample imperfection. The small fraction of incorrectly polarized light, which has negligible influence on the parallel component, could significantly affect the ellipsometric functions for the perpendicular polarization, leading to an offset of the data with respect to those provided by the KK analysis even though the spectral shape is quite satisfactory. In spite of the decrease in the measured reflectivity due to diffusion of light, we have more confidence in the values of $\tilde{n}$ deduced from the KK analysis of the reflectance spectrum along the perpendicular component than in the corresponding data obtained by ellipsometry. This fact is further supported by the consistency between the R and T inversion results and those afforded by the KK analysis.

To the best of our knowledge, there are a limited number of experimental studies that have provided a quantitative determination of the strongly anisotropic optical properties of conjugated polymers by means of different spectroscopic techniques.[39] Due to the complexity of the systems under investigation, it is very difficult to estimate the uncertainty in the absolute values of the optical properties, which also depends on the adopted experimental technique. However, it is generally assumed that the refractive index determined from coherent R and T inversion has a maximum uncertainty of about 5%. The intrinsic error of KK analysis is about 10%, in particular in the region close to the high-energy border of the spectra. We cannot provide an evaluation of the uncertainty for the ellipsometric data due to the complexity of the system under investigation.

Finally, we would like to comment on the polarization properties of the transitions appearing in the high-energy part of the spectrum. From the ε_2 spectra reported in Figs. 5 and 6, it is difficult to directly assess the polarization of the peaks

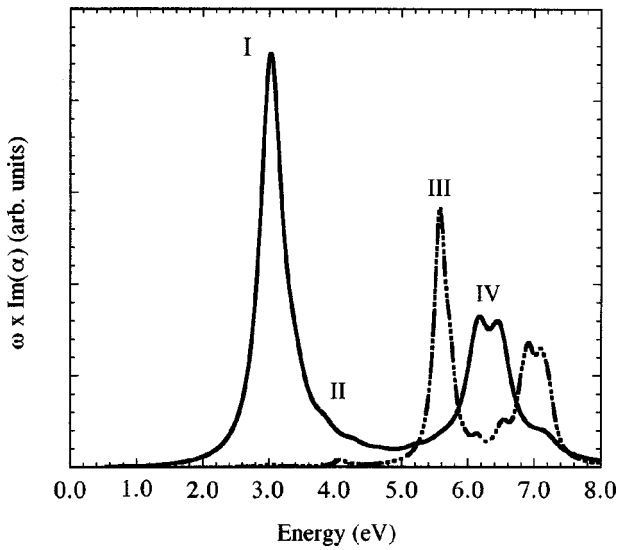

FIG. 7. INDO/SCI-calculated absorption spectrum of an 11-ring PPV oligomer; the solid and dot-dashed lines refer to the parallel and perpendicular polarizations, respectively.

around 4.5 and 4.7 eV due to the presence of a background created by the other optical transitions. Moreover, these two peaks exhibit a small red shift (about 30 meV) when going from the parallel to the perpendicular polarization. After subtraction of the background from the ε_2 spectra, the peaks appear to be more intense in the perpendicular spectrum, thus suggesting a perpendicular polarization for the associated optical transition.

V. THEORY

We have initially optimized the geometry of an eleven-ring PPV oligomer (PPV-11) representative of the corresponding polymer with the help of the semiempirical Hartree-Fock Austin Model 1 (AM1) method,[40] assuming a planar conformation for the conjugated backbone. The transition energies and transition dipole moments of the lowest 200 excited states (up to 7.3 eV) are then calculated by means of the semiempirical Hartree-Fock intermediate neglect of differential overlap (INDO) Hamiltonian (as parametrized by Ridley and Zerner) coupled to a single-configuration-interaction (SCI) scheme.[41] The optical absorption spectrum of the chain is simulated by plugging the INDO/SCI transition energy and transition dipole values into a frequency-dependent sum-over-states (SOS) expression for the imaginary part of the linear polarizability $\tilde{\alpha}$.[42] We simulate the parallel and perpendicular components of the optical absorption spectra from the frequency dispersion of $\omega\,\mathrm{Im}\,\tilde{\alpha}(\omega)$, using the transition dipole moments calculated along the chain axis and the in-plane perpendicular axis, re-

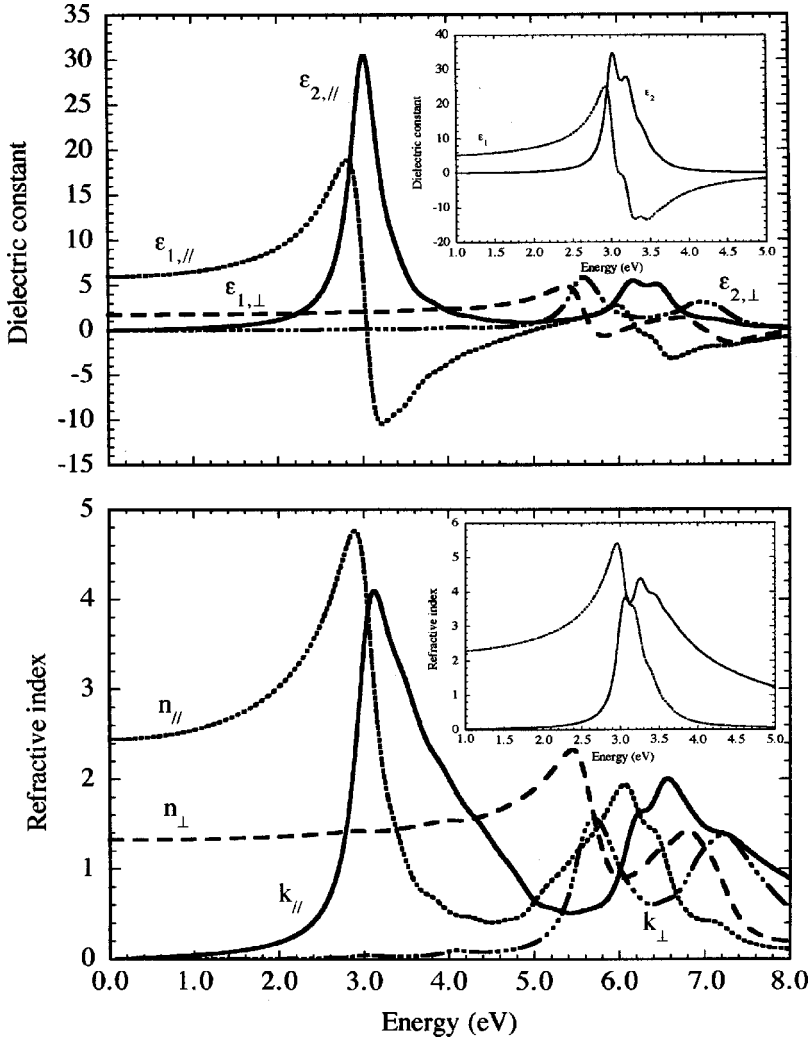

FIG. 8. Upper panel: INDO/SCI-calculated frequency dispersion of the dielectric constant of an 11-ring PPV oligomer [solid line: parallel component of $\varepsilon_2(\omega)$; dotted line: parallel component of $\varepsilon_1(\omega)$; dot-dashed line: perpendicular component of $\varepsilon_2(\omega)$; dashed line: perpendicular component of $\varepsilon_1(\omega)$]. We show in the inset the calculated dispersion of the real and imaginary parts of the parallel component of $\tilde{\varepsilon}(\omega)$ when taking into account only the lowest excited state and the associated vibronic structure [solid line: $\varepsilon_2(\omega)$; dotted line: $\varepsilon_1(\omega)$]. Similar curves are displayed in the lower panel for the refractive index.

spectively (see Fig. 7). As described in our previous study,[30] the calculated spectrum of the fully oriented PPV oligomer within the experimental spectroscopic range is characterized by (i) an intense absorption feature at 3.0 eV (peak I) and a weak shoulder around 3.7 eV (peak II) that are both polarized along the chain axis and originate from a mixing of one-electron excitations between delocalized molecular levels ($d \rightarrow d^*$); (ii) an absorption band around 5.5 eV (peak III) with a dominant perpendicular polarization that results from a mixing of excitations between a localized and a delocalized level ($l \rightarrow d^*$ and $d \rightarrow l^*$); and (iii) a fourth absorption band (peak IV) beyond 6 eV polarized along the chain axis and mostly described by excitations taking place between localized levels ($l \rightarrow l^*$).

Figure 8 reports the calculated frequency dispersion of the real and imaginary parts of the dielectric constant $\tilde{\varepsilon}(\omega)$ and refractive index $\tilde{n}(\omega)$, respectively, for both the parallel and perpendicular components. These simulations are obtained on the basis of the expression $\tilde{\varepsilon}(\omega) = 1 + 4\pi\tilde{\chi}^{(1)}(\omega)$ (in CGS units) and $[\tilde{n}(\omega)]^2 = \tilde{\varepsilon}(\omega)$; the linear susceptibility $\tilde{\chi}^{(1)}(\omega)$ is taken here equal to $N\tilde{\alpha}(\omega)$, where N is the density of PPV-11 chains. We thus neglect local-field effects on the dielectric function[43] but choose the value of N in such a way that the calculated value of the real part of the parallel component of the dielectric constant at the static limit matches the experimental value. This results in an effective value of N equal to $3.17 \times 10^{21}\,\mathrm{cm}^{-3}$ (note that such a value leads to a density of PPV unit cells on the order of $11N = 3.48 \times 10^{22}\,\mathrm{cm}^{-3}$, which is larger than the experimental estimate made from the lattice parameters of crystalline PPV, $6.36 \times 10^{21}\,\mathrm{cm}^{-3}$.[21,44] The theoretical (Fig. 8) and experimental (Figs. 3–6) spectra are observed to be in excellent agreement.

We have also simulated the coupling between vibrational modes and the lowest optical transition of the PPV chains; such coupling is clearly observed for the parallel component in the frequency dispersions of $\tilde{n}$ and $\tilde{\varepsilon}$ (see Figs. 3–6). The corresponding simulations are shown in the insets of Fig. 8, where only the lowest excited state, which is strongly optically coupled to the ground state, has been involved. The vibronic effects have been treated on the basis of the displaced harmonic oscillator model, as detailed in earlier works.[28,45] Using the Franck-Condon approximation, the intensity of an optical transition between the vibronic level $|g,0\rangle$ in the ground state g and the vibronic level $|e,\nu\rangle$ in the lowest excited state e is found to be proportional to (i) the square of the electronic transition dipole moment $\langle g|\mu|e\rangle$; and (ii) the square of the Franck-Condon factor $\langle 0|\nu\rangle$ describing the overlap between the two vibrational wave functions. The latter term is expressed in the harmonic approximation by

$$\langle 0|\nu\rangle^2 = \frac{e^{-S}S^{\nu}}{\nu!}, \tag{5}$$

where S is the Huang-Rhys factor associated with the vibrational mode. In the case of PPV chains, we explicitly consider two effective Raman modes at 0.21 and 0.16 eV; the associated fractional Huang-Rhys factors are taken in a 2/1 ratio (i.e., $S_{\mathrm{total}} = 2S_{0.21} + S_{0.16}$), in agreement with the relative intensities of the two modes in the experimental Raman spectra[28,45] (these values are consistent with the Raman spectra reported in the present study). We have previously estimated the total Huang-Rhys factor S_{total} of highly conjugated PPV to be 0.7; this estimate was made from a linear extrapolation of the values obtained when fitting the vibronic structure observed in the highly resolved photoluminescence spectra of PPV oligomers containing from 2 to 5 rings and dispersed in an inert matrix.[45] This choice of Huang-Rhys factor leads to a remarkable reproduction of the relative intensities of the 0-0 and 0-1 vibronic features of the lowest absorption band of PPV in the frequency dispersion of $\tilde{\varepsilon}$ (see Fig. 5); this agreement confirms the highly delocalized nature of the PPV backbones under study. The larger intensity of the 0-0 peak has also been reported in previous experimental studies of highly conjugated PPV's;[46,47] this contrasts with the spectra of very short oligomers where the lowest two vibronic peaks have similar intensities.[45] Both the experimental and simulated spectra also display a shoulder on the high-energy side of the lowest absorption band that we assign to the 0-2 vibronic transition. Interestingly, the calculations agree with the experimental data in that the relative intensities of lowest two vibronic satellites are reversed when plotting the frequency dispersion of the imaginary part of the refractive index. The fine structure observed in the low-energy region of the frequency dispersion of the real part of $\tilde{n}$ and $\tilde{\varepsilon}$ is also remarkably well reproduced by the simulations.

VI. DISCUSSION

This work reports a detailed characterization in a wide spectral range of the complex optical constants and their polarization properties in highly stretch-oriented PPV. Such data were not previously available in the literature since the refractive index has been traditionally described in the energy range below the absorption edge, i.e., in the spectral region of photoluminescence[3–5,7,8] and light guiding.[48–50] The values of the refractive index reported for unoriented films of soluble PPV derivatives used in optical devices vary between 1.5 and 1.8 in their transparent region. Anisotropic optical behavior is sometimes observed due to the preferential deposition of the chains on the substrate.[3,51] Such values are slightly lower than the average refractive index $\langle n\rangle$ [$\langle n\rangle = (n_1 + 2n_\perp)/3$] estimated from our data (see Figs. 3 and 4). This effect can be attributed to an increase in the chain density when going from substituted to unsubstituted PPV backbones; in other words, this implies that the number of PPV monomers per volume unit decreases upon substitution, thus reducing the macroscopic π-electron density. In contrast, the anisotropy and dispersion properties of the refractive index in the 600–800-nm spectral range of the PPV samples reported in Ref. 49 are in good quantitative agreement with our results. The value of $\langle n\rangle$ and its dispersion also matches the data reported in Refs. 52 and 53 for isotropic PPV thin films. We thus conclude that, as expected, the derivatization of the PPV backbone by electroactive side groups, modulates not only the processability but also the electronic and optical properties of the material.

Similarly, only a few experimental studies based on optical[52] and EELS[38] measurements have described the optical constants of PPV above the absorption threshold. The optical data obtained for unoriented samples[52] appear to be underestimated for both the real and imaginary parts with

respect to the present results averaged over the two polarization components. It is not straightforward to make a direct comparison between our data and the EELS spectra since significant differences are expected in the shape and absolute energies of the optical features.[54] As a matter of fact, the lowest optical absorption peak in our samples is redshifted by more than 0.5 eV and the high-energy bands have a reduced relative oscillator strength when compared to the corresponding features in the $\tilde{\varepsilon}$ spectra deduced from EELS measurements obtained for a small momentum transfer (0.1 $Å^{-1}$).[38] Moreover, the optical transition at 3.7 eV is masked by the lowest absorption band and the vibronic replicas cannot be resolved in the EELS spectra.[38] We believe that the differences observed in the optical properties are due to the chemical and morphological quality of the two samples and not to the different techniques used for their characterization.

The theoretical simulations confirm that the fine structure observed in the low-energy range of the frequency dispersion of the optical constants originate from vibronic effects that can be described within the Franck-Condon approximation.[28,45] The spacings between the vibronic replicas in the reflectance spectrum are 0.22 and 0.25 eV, thus larger than that in the optical absorption spectra reported in Ref. 28, which were simulated by the use of two effective modes at 0.16 and 0.21 eV. This probably originates from the mixing of the real and imaginary parts of the refractive index when calculating the reflectivity spectrum. More relevant values close to 0.2 eV are obtained from the ε_2 spectra corresponding to the optical function directly connected to the electronic structure of the material. Approximate values of the energy of the phonons coupled to the lowest optical absorption can also be determined from the Raman spectrum reported in Fig. 2 or in the literature.[55] However, the best estimates of these parameters are obtained only from the study of the excitation profiles of the resonant Raman effect.[56] The frequencies of the Raman modes reported in this study agree very well with those reported for other oriented PPV's[33,34] and further confirm the very good orientation of the polymer chains along the stretching direction.

The small feature appearing just below the edge ($\sim$2.2 eV) of the lowest absorption band in the parallel reflectance spectrum (which has no counterpart in the corresponding transmittance spectrum) is not observed in the ε_2 dispersion spectra. Therefore, this feature cannot be assigned to an electronic transition and probably results from processes linked to light reflection at the backside when the sample is still transparent. At the absorption edge, the attenuation of this effect (from 2.1 to 2.2 eV the absorption coefficient increases from 202 to 348 cm^{-1}) leads to a decrease in the measured signal, leading to the appearance of the small feature in the reflectance spectrum. This effect allows for the determination of the onset of the lowest absorption edge due to the longer chains in highly oriented PPV to be around 2.2 eV.

The polarization and relative intensities of the absorption bands in the ε_2 spectra of our highly stretched oriented-PPV samples and those reported for oriented MEH-PPV (Ref. 31) provide a good basis for discussing the nature of the electronic transitions in PPV and its substituted derivatives. According to the peak labeling introduced in Sec. V, we will describe the experimental absorption spectrum of PPV by referring to peak I for the lowest absorption band and peaks II, III, and IV for the bands around 3.7, 4.7, and 6.0 eV, respectively. There is an overall agreement among theoretical studies that peak I originates from π-π^* transitions between delocalized levels.[16–28] Both our experimental and theoretical spectra show that this absorption feature is much broader in the n spectrum ($\sim$2.0 eV) than in the ε spectrum ($\sim$1.0 eV), thus preventing peak II to be unambiguously detected from the n spectra.

Most of the theoretical studies indicate that peak III originates from $l \rightarrow d^*/d \rightarrow l^*$ transitions and has a dominant polarization perpendicular to the chain axis while peak IV results from $l \rightarrow l^*$ excitations and is polarized parallel to the chain axis.[16–28] The general agreement between all the theoretical studies for the latter two peaks contrasts with recent calculations of the optical excitations in PPV based on one-particle and two-particle Green's functions, which give no evidence for a relatively intense optical transition around 5 eV with a perpendicular polarization.[57] According to both the INDO/SCI calculations and other theoretical works,[58] the excited states giving rise to the third absorption band have a pronounced intrachain (and interchain) charge-transfer character, which has been invoked to rationalize the steady-state photocurrent action spectra of PPV and substituted derivatives.[18] The interchain charge-transfer character of this band might also explain the increased interchain carrier hopping rate responsible for the high carrier lifetime evidenced by ultrafast photoinduced infrared activated vibrations measurements when pumping with a photon energy close to that of peak III.[59]

The INDO/SCI calculations suggest that the shoulder observed in the reflectance spectrum of unsubstituted PPV around 3.7 eV corresponds to an optical transition between delocalized levels ($d \rightarrow d^*$), which is induced by finite-size effects and polarized along the chain axis, in agreement with the experimental data.[30] The quantum-chemical calculations reported in Refs. 19 and 26 indicate that the intensity of this peak decreases when chain length is increased. The optical absorption spectra of substituted PPV chains have a very similar shape when compared to those of unsubstituted chains. However, alkoxy-substituted derivatives are further characterized by the appearance around 3.7 eV of new absorption peaks mostly described by $l \rightarrow d^*/d \rightarrow l^*$ excitations, due to the breaking of the charge conjugation symmetry (CCS) upon attachment of electroactive substituents on the PPV backbone.[19,25,27] The main effect of the alkoxy groups is actually to decrease the separation between the energies of the lowest $l \rightarrow d^*/d \rightarrow l^*$ and $d \rightarrow d^*$ excitations and thus to enhance the strength of the interaction between the two types of excitations. This allows for an efficient intensity borrowing from the lowest absorption band that contributes to the intensity of peak II, which is also expected to decrease for growing chain length.[19] Interestingly, quantum-chemical calculations show that the transition dipole moment of these new peaks is almost exclusively governed by their weak $d \rightarrow d^*$ character (i.e., the contributions of the $l \rightarrow d^*/d \rightarrow l^*$ excitations tend to cancel each other), thus yielding a polarization along the chain axis.[19] Recently, Martin *et al.*[60] suggested that CCS breaking could also play a role in unsubstituted PPV chains due to the presence of defects. This interpretation is actually quite consistent with the present discussion; indeed, defects are expected to amplify

finite-size effects when leading to simple breaks in conjugation and/or to induce CCS breaking when introducing new electroactive moieties (such as carbonyl groups) attached to the PPV segments.

The energy separation between the constructive (peak III) and destructive (peak II) interactions of the $l \rightarrow d^*/d \rightarrow l^*$ excitations is larger than 1.0 eV in the INDO/SCI calculations. This contrasts with recent theoretical studies by Kirova, Brazovski, and co-workers where the band structure of unsubstituted PPV is first generated and subsequently corrected to include Coulomb attraction between electron and hole;[16,17] peak II in the spectrum of an alkoxy-substituted five-ring PPV oligomer is assigned by these authors to excitonic features resulting from both destructive and constructive interactions among the $l \rightarrow d^*/d \rightarrow l^*$ excitations, which are calculated to be separated by $\sim$0.1 eV, and it is predicted to be perpendicularly polarized in contrast with the experimental data reported here and in Refs. 30 and 31. The third absorption band is then associated to the interband (i.e., without Coulomb attraction between electron and hole) transition from $l \rightarrow d^*/d \rightarrow l^*$ levels. From the previous considerations, we stress that a description of the optical transitions of an alkoxy-substituted oligomer based on the results of calculations performed on the unsubstituted chain is misleading. It is also difficult to believe that free carriers can be generated through an interband transition in such very short chain segments. The band model developed in Refs. 16 and 17 yields a binding energy on the order of 0.8–0.9 eV for the excitons generated in band II of PPV, much larger than the maximum value of about 0.3 eV discussed in Ref. 61 for excitons generated in band I, which are similar in nature to those associated to band II, according to the analysis of the excited-state wave functions of PPV chains performed at the INDO/SCI level.[18] It is also worth stressing that the quantum-chemical calculations reported here on the PPV oligomers demonstrate that an approach such as ours is suitable to describe the absorption spectrum of very long conjugated chains.

Miller *et al.* have recently reported the polarized absorption spectra of highly stretch-oriented MEH-PPV, aligned in ultrahigh-molecular-weight polyethylene.[31] Both the MEH-PPV samples studied in Ref. 31 and our PPV samples are highly oriented and show a higher anisotropy in their optical properties than that reported in previous works.[19] In PPV, peak I is polarized parallel to the chain axis, as is the case for peak II, which has a *vanishingly* small intensity; this can be related to the highly delocalized nature of the PPV chains under study, which tends to reduce the intensity of peak II.[19,25] Peak III has contributions from both polarizations but appears to have a larger perpendicular component. The polarization assignments of the peaks in the PPV spectrum are fully supported by the results of the INDO/SCI calculations. Peaks I, II, and IV in the absorption spectrum of MEH-PPV are also found to be polarized parallel to the chain direction while peak III has a perpendicular orientation;[31] this is again in full agreement with the INDO/SCI calculations. We emphasize that the dominant polarization of peaks III and IV cannot be readily assessed from the relative intensities of the parallel and perpendicular components observed in the polarized spectra, since the measured polarization ratio of the two peaks is affected by their mutual overlap. Further signal processing is thus required before getting an estimate of the true ratio; moreover, the value of the polarization ratio can also be affected by small chain misalignments within the samples. We also note that, in contrast to the results of the INDO/SCI calculations, the dominant polarization for peak II of MEH-PPV is given as perpendicular in Refs. 16 and 25; this spurious result is related to the fact that the coupling between one-electron transitions polarized parallel and perpendicular to the chain axis is not taken into account in these models.

The polarized optical absorption spectra of highly oriented PPV and MEH-PPV films are thus measured to be quite similar; however, two fundamental differences are present:

(i) The relative intensity of peak I with respect to that of all the other peaks is much larger in PPV than in MEH-PPV.[31] This is likely a result of a redistribution of the intensity of the high-energy optical features of PPV into many new components in the substituted derivative, upon breaking the charge-conjugation symmetry;

(ii) peak II, which has a parallel polarization in both cases, has a much weaker intensity in oriented PPV than in oriented MEH-PPV.[31] This difference could originate from changes in the effective conjugation length (this is expected, for instance, if the PPV chains are more planar than those of MEH-PPV) and/or from a different impact of finite-size effects on the distinct physical mechanisms responsible for the generation and oscillator strength of peak II in the two polymers. However, in both cases, the intensity should be very weak for very long chains according to the calculations in Ref. 19.

In conclusion, we have reported an extensive determination of the anisotropic optical functions of highly stretch-oriented PPV in a wide spectral range by using reflectance, transmittance, and ellipsometry measurements. The frequency dispersion of the complex optical functions of PPV has also been computed by means of correlated quantum-chemical calculations. A very good agreement is observed between the experimental and theoretical spectra and opens the way towards an unified description of the nature and polarization of the optical transitions in PPV and alkoxy-substituted derivatives. Further investigations of the optical properties of oriented substituted and unsubstituted PPV chains with well-defined conjugation lengths are highly desirable to confirm our interpretation.

ACKNOWLEDGMENTS

We thank Dr. Ohnishi and Dr. T. Noguchi for providing us the PPV samples. We thank Dr. E. K. Miller for providing us his data on oriented MEH-PPV before their publication. We acknowledge helpful discussion with Dr. M. Patrini on the ellipsometric measurements. We also thank Instrument S.A. Italy for allowing us the use of their micro Raman spectrometer. The work in Genova is supported by the Italian Ministry of University and Technological Research (MURST) and by the National Research Council (CNR). The work in Mons is supported by the Belgian Federal Government ''Pôle d'Attraction Interuniversitaire en Chimie Supramoléculaire et Catalyse, PAI 4/11'' and the Belgian National Fund for Scientific Research (FNRS). J.C. received support from FNRS.

[1] See, for instance, the *Proceedings of the International Conference of Science and Technology of Synthetic Metals, Montpellier, France*, Synth. Met. **101**, 1–3 (1999).
[2] R. H. Friend, J. H. Burroughes, and T. Shimoda, Phys. World **35**, (1999).
[3] M. D. McGehee, R. Gupta, S. Veenstra, E. K. Miller, M. A. Dìaz-Garcìa, and A. J. Heeger, Phys. Rev. B **58**, 7035 (1998).
[4] S. V. Frolov, Z. V. Vardeny, and K. Yoshino, Phys. Rev. B **57**, 9141 (1998).
[5] S. V. Frolov, Z. V. Vardeny, and K. Yoshino, Appl. Phys. Lett. **72**, 1802 (1998).
[6] V. G. Kozlov, G. Parthasarathy, P. E. Burrows, S. R. Forrest, Y. You, and M. E. Thompson, Appl. Phys. Lett. **72**, 144 (1998).
[7] S. V. Frolov, M. Shkunov, Z. V. Vardeny, and K. Yoshino, Phys. Rev. B **56**, R4363 (1997).
[8] F. Hide, M. A. Díaz-García, B. J. Schwartz, and A. J. Heeger, Acc. Chem. Res. **30**, 430 (1997).
[9] V. G. Kozlov, V. Bulovic, and S. R. Forrest, Appl. Phys. Lett. **71**, 2575 (1997).
[10] C. Zenz, W. Graupner, S. Tasch, G. Leising, K. Müllen, and U. Sherf, Appl. Phys. Lett. **71**, 2566 (1997).
[11] V. G. Kozlov, V. Bulovic, P. E. Burrows, and S. R. Forrest, Nature (London) **389**, 363 (1997).
[12] N. Tessler, G. J. Denton, and R. H. Friend, Nature (London) **382**, 695 (1996).
[13] N. C. Greenham, R. H. Friend, and D. D. C. Bradley, Adv. Mater. **6**, 491 (1994); A. Dodabalapur, Solid State Commun. **102**, 259 (1997).
[14] H. F. Wittmann, J. Grüner, R. H. Friend, G. W. C. Spencer, S. C. Moratti, and A. B. Holmes, Adv. Mater. **7**, 541 (1995).
[15] I. D. W. Samuel, G. Rumbles, and R. H. Friend, in *Primary Photoexcitations in Conjugated Polymers: Molecular Exciton Versus Semiconductor Band Model*, edited by N. S. Sariciftci (World Scientific, Singapore, 1997), p. 140.
[16] N. Kirova, S. Brazovskii, and A. R. Bishop, Synth. Met. **100**, 29 (1999).
[17] S. Brazovskii, N. Kirova, A. R. Bishop, V. Klimov, D. McBranch, N. N. Barashkov, and J. P. Ferraris, Opt. Mater. **9**, 472 (1998).
[18] A. Köhler, D. A. dos Santos, D. Beljonne, Z. Shuai, J. L. Brédas, A. B. Holmes, A. Kraus, K. Müllen, and R. H. Friend, Nature (London) **392**, 903 (1998).
[19] M. Chandross, S. Mazumdar, M. Liess, P. A. Lane, Z. V. Vardeny, M. Hamaguchi, and K. Yoshino, Phys. Rev. B **55**, 1486 (1997).
[20] M. Chandross and S. Mazumdar, Phys. Rev. B **55**, 1497 (1997).
[21] C. Ambrosch-Draxl and R. Abet, Synth. Met. **85**, 1099 (1997).
[22] Y. Shimoi and S. Abe, Synth. Met. **78**, 219 (1996).
[23] J. Cornil, D. A. dos Santos, D. Beljonne, and J. L. Brédas, J. Phys. Chem. **99**, 5604 (1995).
[24] M. Fahlman, M. Lögdlund, S. Stafström, W. R. Salaneck, R. H. Friend, P. L. Burn, A. B. Holmes, K. Kaeriyama, Y. Sonoda, O. Lhost, F. Meyers, and J. L. Brédas, Macromolecules **28**, 1959 (1995).
[25] Y. N. Gartstein, M. J. Rice, and E. M. Conwell, Phys. Rev. B **51**, 5546 (1995).
[26] M. J. Rice and Y. N. Gartstein, Phys. Rev. Lett. **73**, 2504 (1994); Y. N. Gartstein, M. J. Rice, and E. M. Conwell, Phys. Rev. B **52**, 1683 (1995).
[27] J. Cornil, D. Beljonne, R. H. Friend, and J. L. Brédas, Chem. Phys. Lett. **223**, 82 (1994).
[28] J. Cornil, D. Beljonne, Z. Suhai, T. W. Hagler, I. Campbell, D. D. C. Bradley, J. L. Brédas, C. W. Spangler, and K. Mullen, Chem. Phys. Lett. **247**, 425 (1995).
[29] D. Yaron, E. E. Moore, Z. Shuai, and J. L. Brédas, J. Chem. Phys. **108**, 7451 (1998).
[30] D. Comoretto, G. Dellepiane, D. Moses, J. Cornil, D. A. dos Santos, and J. L. Brédas, Chem. Phys. Lett. **289**, 1 (1998).
[31] E. K. Miller, D. Yoshida, C. Y. Yang, and A. J. Heeger, Phys. Rev. B **59**, 4661 (1999).
[32] S. Kuroda, T. Noguchi, and T. Ohnishi, Phys. Rev. Lett. **72**, 286 (1994), and references therein.
[33] J. Orion, J. P. Buisson, and S. Lefrant, Phys. Rev. B **57**, 7050 (1998); E. Mulazzi, A. Ripamonti, J. Wery, B. Dulieu, and S. Lefrant, *ibid.* **60**, 16 519 (2000).
[34] S. Webster and D. N. Batchelder, Polymer **37**, 4961 (1996).
[35] O. S. Heavens, *Optical Properties of Thin Films* (Butterworths Scientific, London, 1955).
[36] H. Röeseler, *Infrared Spectroscopic Ellipsometry* (Akademie, Berlin, 1990).
[37] F. Wooten, *Optical Properties of Solids* (Academic, New York, 1972).
[38] E. Pellegrin, J. Fink, J. H. F. Martens, D. D. C. Bradley, H. Murata, S. Tokito, T. Tsutsui, and S. Saito, Synth. Met. **41–43**, 1353 (1991).
[39] M. R. Drury and D. Bloor, J. Phys. D **23**, 108 (1990).
[40] M. J. S. Dewar, E. G. Zoebisch, E. F. Healy, and J. J. P. Stewart, J. Am. Chem. Soc. **107**, 3902 (1985).
[41] J. Ridley and M. C. Zerner, Theor. Chim. Acta **32**, 111 (1973).
[42] B. J. Orr and J. F. Ward, Mol. Phys. **20**, 513 (1971).
[43] D. Comoretto, G. Dellepiane, G. F. Musso, R. Tubino, R. Dorsinville, A. Walser, and R. R. Alfano, Phys. Rev. B **46**, 10 041 (1992), and references therein.
[44] D. Chen, M. J. Winokur, M. A. Masse, and F. Karasz, Phys. Rev. B **41**, 6759 (1990).
[45] J. Cornil, D. Beljonne, C. M. Heller, I. H. Campbell, B. K. Laurich, D. L. Smith, D. D. C. Bradley, K. Müllen, and J. L. Brédas, Chem. Phys. Lett. **278**, 139 (1997).
[46] K. Pichler, D. A. Halliday, D. D. C. Bradley, P. L. Burn, R. H. Friend, and A. B. Holmes, J. Phys.: Condens. Matter **5**, 7155 (1993).
[47] C. L. Gettinger, A. J. Heeger, J. M. Drake, and D. J. Pine, J. Phys. Chem. **101**, 1673 (1994).
[48] R. Burzynski, P. N. Prasad, and F. E. Karasz, Polymer **31**, 627 (1991).
[49] J. Swiatkiewicz, P. N. Prasad, and F. E. Karasz, J. Appl. Phys. **74**, 525 (1993).
[50] T. Gabler, R. Waldhausl, A. Bräuer, F. Michelotti, H.-H. Hörhold, and U. Bartuch, Appl. Phys. Lett. **70**, 928 (1997).
[51] J. Sturm, S. Tasch, A. Niko, G. Leising, E. Toussaere, J. Zyss, T. C. Kowalczyk, K. D. Singer, U. Scherf, and J. Huber, Thin Solid Films **298**, 138 (1997); W. M. V. Wan, N. C. Greenham, and R. H. Friend, J. Appl. Phys. **87**, 2542 (2000); W. M. V. Wan, R. H. Friend, and N. C. Greenham, Thin Solid Films **363**, 310 (2000).
[52] A. Mathy, K. Ueberhofen, R. Schenk, H. Gregorious, R. Garay, K. Müllen, and C. Bubeck, Phys. Rev. B **53**, 4367 (1996).
[53] P. K. H. Ho, D. S. Thomas, R. H. Friend, and N. Tessler, Science **285**, 233 (1999).
[54] E. Zojer, Z. Shuai, G. Leising, and J. L. Brédas, J. Chem. Phys. **111**, 1668 (1999).
[55] S. Heun, R. F. Mahrt, A. Greiner, U. Lemmer, H. Bässler, D. A. Halliday, D. D. C. Bradley, P. L. Burn, and A. B. Holmes, J.

Phys.: Condens. Matter **5**, 247 (1993).
[56] R. S. Cataliotti, G. Paliani, G. Dellepiane, S. Fuso, S. Destri, L. Piseri, and R. Tubino, J. Chem. Phys. **82**, 2223 (1985).
[57] M. Rohlfing and S. G. Louie, Phys. Rev. Lett. **82**, 1959 (1999).
[58] S. Mukamel, S. Tretiak, T. Wagersreiter, and V. Chernyak, Science **277**, 781 (1997).
[59] D. Moses, A. Dogariu, and A. J. Heeger, Phys. Rev. B **61**, 9373 (2000); Chem. Phys. Lett. **316**, 354 (2000).
[60] S. J. Martin, H. Mellor, D. D. C. Bradley, and P. L. Burn, Opt. Mater. **9**, 88 (1998); S. J. Martin, D. D. C. Bradley, P. A. Lane, H. Mellor, and P. L. Burn, Phys. Rev. B **59**, 15 133 (1999).
[61] J. L. Brédas, J. Cornil, and A. J. Heeger, Adv. Mater. **8**, 447 (1996).